

Higher Order Discontinuous Galerkin Methods for Flow and Transport in Porous Media

Peter Bastian

Interdisziplinäres Zentrum für Wissenschaftliches Rechnen, Universität Heidelberg, Im Neuenheimer Feld 348, 69120 Heidelberg, Germany

Abstract. In this paper we describe higher order discontinuous Galerkin (DG) methods for application in subsurface transport. Based on a scheme developed by Oden, Babuška and Baumann we present a method for the solution of the elliptic flow equation and describe a multigrid method for the fast solution of the arising algebraic equations. For the solution of the transport equation we combine the DG space discretization with higher order explicit Runge-Kutta schemes in the convection-dominated case and with diagonally implicit Runge-Kutta schemes in the diffusion-dominated case. Numerical results are presented for single-phase flow in heterogeneous media, solute transport and two-phase flow.

1 Introduction

In this paper we are interested in the accurate numerical solution of the equations describing the flow of fluids and dissolved components in the subsurface.

Let Ω be a domain in \mathbb{R}^d , $d = 2, 3$, with outward unit normal n . The equation for groundwater flow in head-based formulation is given by

$$\nabla \cdot u = f \quad \text{in } \Omega, \quad u = -K\nabla H, \quad (1)$$

with Dirichlet boundary conditions $H = H_0$ on Γ_H and flux boundary conditions $u \cdot n = U$ on boundary Γ_U . H is the hydraulic head, u is the Darcy velocity and K is the permeability tensor.

The challenge for numerical methods solving (1) is to achieve high accuracy for the flow velocity u subsequently entering the transport equation. Moreover, the permeability tensor may vary over many orders of magnitude.

The generic transport equation including convective and dispersive transport, radioactive decay and a reaction term reads

$$R\Phi \left(\frac{\partial C}{\partial t} + \lambda C \right) + \nabla \cdot j = q(C) \quad \text{in } \Omega, \quad j = uC - D(u)\nabla C \quad (2)$$

with Dirichlet boundary conditions $C = C_0$ on Γ_C , flux boundary conditions $j \cdot n = J$ on boundary Γ_J and outflow boundary conditions $j \cdot n = (uC - D(u)\nabla C) \cdot n$ on Γ_O . We assume that $u \cdot n \geq 0$ on Γ_O . R is the retardation factor, Φ the effective porosity, $\lambda = \log 2/T$ with T the half life time of the element and D the diffusion/dispersion tensor.

The flow equation (1) is of elliptic type while the transport equation (2) is of hyperbolic type if $D = 0$ and parabolic otherwise.

A nonlinear extension of the equations above describes the flow of two incompressible and immiscible fluids, e. g. water (the wetting phase w) and oil (the non-wetting phase n), in a porous medium. The primary unknowns are the pressure of the water phase p_w and the saturation of the non-wetting phase S_n . For details of the modeling we refer to [28,4,24].

The phase pressure equation is given by

$$\nabla \cdot u = q \quad \text{in } \Omega, \quad u = -\lambda K(\nabla p_w - G) - \lambda_n K \nabla p_c \quad (3)$$

with boundary conditions

$$p_w = p_{wd} \text{ on } \Gamma_{wd}, \quad u \cdot n = U \text{ on } \Gamma_{wn}, \quad (4)$$

and the total velocity $u = u_w + u_n$ being the sum of the phase velocities, K the absolute permeability, q the source term, $k_{rw}(1 - S_n), k_{rn}(S_n)$ the relative permeabilities, $p_c(1 - S_n)$ the capillary pressure function, μ_w, μ_n the dynamic viscosities of the two fluids, $\lambda_w = k_{rw}(1 - S_n)/\mu_w, \lambda_n = k_{rn}(S_n)/\mu_n$ the phase mobilities, $\lambda = \lambda_w + \lambda_n$ the total mobility, ϱ_w, ϱ_n the densities of the two fluids and $G = g(\lambda_w \varrho_w + \lambda_n \varrho_n)/\lambda$, where g is a vector that points in the direction of gravity and has the length of the gravitational acceleration.

The phase pressure equation (3) is coupled to the saturation equation

$$\Phi \frac{\partial S_n}{\partial t} + \nabla \cdot j_n = q_n \quad \text{in } \Omega, \quad j_n = f_n(S_n)w(u, S_n) - hK \nabla p_c \quad (5)$$

with boundary and initial conditions

$$S_n = S_{nd} \text{ on } \Gamma_{nd}, \quad j_n \cdot n = \phi_n/\varrho_n \text{ on } \Gamma_{nn}, \quad S_n(t = 0) = S_{n0}, \quad (6)$$

and coefficients

$$f_n = \lambda_n/\lambda, \quad w(u, S_n) = u - \lambda_w(\varrho_w - \varrho_n)Kg, \quad h = \lambda_w \lambda_n/\lambda. \quad (7)$$

For a given function $S_n(x, t)$ the phase pressure equation is elliptic, while for a given total velocity field $u(x, t)$ the saturation equation is either nonlinear hyperbolic if $p_c \equiv 0$ and nonlinear parabolic else.

In this paper we present the application of higher order discontinuous Galerkin (DG) methods to the equations given above. Due to their flexibility, DG methods have been popular among the finite element community and they have been applied to a wide range of computational fluid problems. Since the first DG method introduced in [29] the methods have been developed for hyperbolic problems known as the Runge-Kutta DG method [15,14,11,12,17] and for elliptic problems in [38,27,16,33,34]. A unified analysis for many DG methods for elliptic problems has been given recently in [3]. A general overview is available in [13].

Advantages of DG methods are their higher order convergence property, local conservation of mass and flexibility with respect to meshing and hp -adaptive refinement. Their uniform applicability to hyperbolic, elliptic and parabolic problems as well as their robustness with respect to strongly discontinuous coefficients renders them very attractive for porous medium flow and transport calculations [32,1]. The application of DG methods to a benchmark problem in atomic waste repository simulation is given in [8]. DG methods for elliptic problems are comparable in quality with mixed finite element methods, as will be shown below.

In this work we use a DG formulation due to Oden, Babuška, and Baumann [27] for elliptic problems and combine it with either the explicit Runge-Kutta DG methods from [12,17] or with diagonally implicit Runge-Kutta time discretizations.

This paper is organized as follows: Section 2 introduces the necessary notation, Section 3 presents the DG scheme for the elliptic flow equation while Section 4 describes the DG scheme for hyperbolic and parabolic transport equations. Numerical results for single and two-phase flow problems are presented in Section 5. Finally, conclusions are given in Section 6.

2 Notation

Let $E_h = \{e_1, \dots, e_{n_h}\}$ be a non-degenerate quasi-uniform subdivision of Ω where $e \in E_h$ is a triangle or quadrilateral if $d = 2$ and e is a tetrahedron, pyramid, prism or hexahedron with planar faces if $d = 3$. Let h denote the maximum diameter of the elements in E_h . The domain covered by $e \in E_h$ is denoted by Ω_e and the outward unit normal to Ω_e is n_e . The subdivision does not have to match up at element boundaries (although this is not yet implemented in the code).

The space of polynomial functions of degree r on element $e \in E_h$ is defined by

$$P_r(\Omega_e) = \{w : \Omega_e \rightarrow \mathbb{R} \mid w(x, y) = \sum_{0 \leq a+b \leq r} c_{ab} x^a y^b\}. \quad (8)$$

The extension to three space dimensions is obvious. Note that P_r can be used on triangles (tetrahedra) *and* quadrilaterals (hexahedra). In the implementation P_r is generated from basis polynomials on the reference element. Moreover, we use basis polynomials that are L^2 -orthogonal on the reference elements. This improves the conditioning of the arising matrices and leads to diagonal mass matrices.

The finite element space used in the DG method is defined as

$$V^r(E_h) = \prod_{e \in E_h} P_r(\Omega_e). \quad (9)$$

Note that functions in $V^r(E_h)$ are discontinuous on the so-called internal skeleton Γ_{int} which is defined as

$$\Gamma_{int} = \{\gamma_{e,f} \mid \gamma_{e,f} = \partial\Omega_e \cap \partial\Omega_f \ \forall e, f \in E_h, e \neq f\}. \quad (10)$$

Correspondingly, the external skeleton is defined as

$$\Gamma_{ext} = \{\gamma_e \mid \gamma_e = \partial\Omega_e \cap \partial\Omega \ \forall e \in E_h\}. \quad (11)$$

With each $\gamma_{e,f} \in \Gamma_{int}$ we associate a unit normal n . The orientation can be selected arbitrarily. With any $\gamma_e \in \Gamma_{ext}$ we associate the unit normal n oriented outward to Ω .

For any $x \in \gamma \in \Gamma_{int}$ we denote the jump of a function $v \in V^r(E_h)$ by

$$[v](x) = \lim_{\epsilon \rightarrow 0^+} v(x + \epsilon n) - \lim_{\epsilon \rightarrow 0^+} v(x - \epsilon n). \quad (12)$$

In addition to the jump we also define the average of a function $v \in V^r(E_h)$ at $x \in \gamma \in \Gamma_{int}$:

$$\langle v \rangle(x) = \frac{1}{2} \left(\lim_{\epsilon \rightarrow 0^+} v(x + \epsilon n) + \lim_{\epsilon \rightarrow 0^+} v(x - \epsilon n) \right). \quad (13)$$

3 DG Method for Flow Equation

3.1 Scheme

The DG method due to Oden, Babuška, and Baumann [27] for solving the elliptic problem (1) is given as follows: Find $H_h \in V^r(E_h)$ such that for all $v \in V^r(E_h)$

$$\begin{aligned} & \sum_{e \in E_h} \int_{\Omega_e} (K \nabla H_h) \cdot \nabla v \, dx \\ & + \sum_{\gamma \in \Gamma_{int}} \int_{\gamma} \langle K \nabla v \cdot n \rangle [H_h] - [v] \langle K \nabla H_h \cdot n \rangle \, ds \\ & + \sum_{\gamma \in \Gamma_{ext} \cap \Gamma_H} \int_{\gamma} (K \nabla v \cdot n) H_h - v K \nabla H_h \cdot n \, ds \\ & = \sum_{e \in E_h} \int_{\Omega_e} f v \, dx - \sum_{\gamma \in \Gamma_{ext} \cap \Gamma_U} \int_{\gamma} U v \, ds + \sum_{\gamma \in \Gamma_{ext} \cap \Gamma_H} \int_{\gamma} (K \nabla v \cdot n) H_0 \, ds \end{aligned} \quad (14)$$

which will be abbreviated as

$$a_h(H_h, v) = f_h(v) \quad \forall v \in V^r(E_h). \quad (15)$$

Note that the Dirichlet boundary condition is approximated weakly. Assuming that the solution is sufficiently regular the convergence rate of the scheme

in the energy norm (and thus for the velocity $u = -K\nabla H$) is $O(h^r)$ and the convergence rate in L^2 is $O(h^r)$ if r is even and $O(h^{r+1})$ if r is odd. This anomaly can be remedied with other stabilizations such as the nonsymmetric interior penalty DG method [30,34] or the local DG method [16,3].

The local conservation property of the DG scheme becomes obvious when a test function $v \in V^r(E_h)$ is inserted which is constant on each element. Then the scheme reduces to

$$\sum_{\gamma \in \Gamma_{int}} \int_{\gamma} [v] \langle u \cdot n \rangle ds + \sum_{\gamma \in \partial\Omega} \int_{\gamma} u \cdot n v ds = \sum_{e \in E_h} \int_{\Omega_e} f v dx \quad (16)$$

which shows that the conserved flux is the average $\langle u \cdot n \rangle$.

3.2 Variational Multigrid Formulation

Insertion of a basis representation into (14) results into a large system of linear equations. Since the underlying problem is elliptic it should be possible to construct optimal order multigrid solvers. Such an algorithm has been presented in [9]. For an introduction to multigrid methods we refer to [21,22]

Here, we will derive the coarse grid correction of a two-grid method in variational form. Let E_0, E_1, \dots, E_J be a nested mesh hierarchy. Let $H_l^{old} \in V^r(E_l)$ be an approximate solution of (14) on mesh level l . We seek a coarse grid correction $c_{l-1} \in V^r(E_{l-1})$ that removes the low frequency errors from H_l^{old} . The subspace correction approach [39] results in the following procedure for the coarse grid correction: Solve

$$a_{l-1}(c_{l-1}, v_{l-1}) = f_h(v_{l-1}) - a_{l-1}(H_l^{old}, v_{l-1}) \quad \forall v_{l-1} \in V^r(E_{l-1}) \quad (17)$$

and correct

$$H_l^{new} = H_l^{old} + c_{l-1}. \quad (18)$$

Note that polynomials of degree r are used also on the coarse grid. This should not be necessary since low frequency errors can be represented with low-order polynomials but on the other hand it does not harm the overall complexity and eases implementation.

In the multigrid algorithm, the exact coarse grid correction (17) is replaced by a recursive application of the same procedure. The entries of the restriction and prolongation matrices are obtained from the equation $\varphi_{i,l-1} = \sum_j \omega_{i,j} \varphi_{j,l}$ stating that every coarse grid basis function $\varphi_{i,l-1}$ can be represented by a linear combination of fine grid basis functions $\varphi_{j,l}$. This follows from the fact that the DG spaces are nested: $V^r(E_{l-1}) \subset V^r(E_l)$. The factors $\omega_{i,j}$ are the entries of the prolongation matrix, see [9] for details.

It remains to specify the smoothing iteration. There, we use a zero order incomplete LU decomposition applied to a blocked matrix where all degrees of freedom associated with one element are collected in a block. Blockwise Jacobi and Gauß-Seidel methods (with respect to the same blocking) are

not effective as smoothers since errors on the internal skeleton Γ_{int} are not removed.

Numerical results for this multigrid algorithm are presented below.

3.3 BDM Projection

The Darcy velocity $u^{DG} = -K\nabla H_h$ computed from $H_h \in V^r(E_h)$ is discontinuous at element boundaries and does not have continuous normal component $u^{DG} \cdot n$. Thus, the average flux $\langle u \cdot n \rangle$ is inconsistent with the fluxes evaluated from left and right. Mathematically we have $u^{DG} \notin H(\text{div}; \Omega)$. A velocity field with continuous normal component is, however, required by most transport simulations such as the scheme described below. In [10] we describe a simple projection scheme $\Pi : (V^r(E_h))^d \rightarrow H(\text{div}; \Omega)$ and prove that this projection does not reduce the accuracy of the DG scheme. This projected velocity $u^* = \Pi(u^{DG})$ will be used in the transport simulation.

4 DG for Transport Equation

4.1 Scheme

The semi-discrete DG scheme for solving the transport equation (2) in either its hyperbolic or parabolic form is given as follows: Find $C_h : [0, T] \rightarrow V^r(E_h)$ such that for all $v \in V^r(E_h)$

$$\begin{aligned}
& \frac{\partial}{\partial t} \sum_{e \in E_h} \int_{\Omega_e} R\Phi C_h v \, dx + \sum_{e \in E_h} \int_{\Omega_e} R\Phi \lambda C_h v \, dx \\
& - \sum_{e \in E_h} \int_{\Omega_e} (u C_h - D\nabla C_h) \cdot \nabla v \, dx + \sum_{\gamma \in \Gamma_{int}} \int_{\gamma} [v] C_h^* \langle u \cdot n \rangle \, ds \\
& + \sum_{\gamma \in \Gamma_{int}} \int_{\gamma} \langle D\nabla v \cdot n \rangle [C_h] - [v] \langle D\nabla C_h \cdot n \rangle \, ds \\
& + \sum_{\gamma \in \Gamma_{ext} \cap \Gamma_C} \int_{\gamma} D\nabla v \cdot n C_h - v D\nabla C_h \cdot n \, ds + \sum_{\gamma \in \Gamma_{ext} \cap \Gamma_C^{out}} \int_{\gamma} v C_h u \cdot n \, ds \\
& + \sum_{\gamma \in \Gamma_{ext} \cap \Gamma_O} \int_{\gamma} v C_h u \cdot n - v D\nabla C_h \cdot n \, ds + J_0^{\sigma, \beta}(C_h, v) \tag{19} \\
& = \sum_{e \in E_h} \int_{\Omega_e} qv \, dx - \sum_{\gamma \in \Gamma_{ext} \cap \Gamma_J} \int_{\gamma} Jv \, ds - \sum_{\gamma \in \Gamma_{ext} \cap \Gamma_C^{in}} \int_{\gamma} v C_0 u \cdot n \, ds \\
& + \sum_{\gamma \in \Gamma_{ext} \cap \Gamma_C} \int_{\gamma} D\nabla v \cdot n C_0 \, ds + \sum_{\gamma \in \Gamma_{ext} \cap \Gamma_C} \frac{\sigma}{|\gamma|^\beta} \int_{\gamma} C_0 v \, ds
\end{aligned}$$

where we have used the refined decomposition of the boundary into Dirichlet outflow

$$\Gamma_C^{out} = \{x \in \Gamma_C \mid u(x) \cdot n > 0\} \quad (20)$$

and Dirichlet inflow

$$\Gamma_C^{in} = \{x \in \Gamma_C \mid u(x) \cdot n \leq 0\} \quad (21)$$

and the interior penalty term [38,30]

$$J_0^{\sigma,\beta}(C, v) = \sum_{\gamma \in \Gamma_{int}} \frac{\sigma}{|\gamma|^\beta} \int_\gamma [C][v] ds + \sum_{\gamma \in \Gamma_{ext} \cap \Gamma_C} \frac{\sigma}{|\gamma|^\beta} \int_\gamma C v ds \quad (22)$$

with user-defined parameters σ and β . This additional penalty term can be used to improve continuity of the solution at internal boundaries.

The concentration in the convective term for $x \in \gamma \in \Gamma_{int}$ is upwinded via

$$C_h^*(x) = \begin{cases} \lim_{\epsilon \rightarrow 0^+} C_h(x - \epsilon n) & \text{if } \langle u \cdot n \rangle \geq 0 \\ \lim_{\epsilon \rightarrow 0^+} C_h(x + \epsilon n) & \text{else} \end{cases} . \quad (23)$$

In the scheme (19) we use the projected velocity u^* defined in Subs. 3.3. The spatial error of this formulation is $O(h^{r+1})$ in L^2 in the hyperbolic case ($D = 0$) for a sufficiently regular solution. Error estimates are provided in [31].

A nice property of the DG method is the correct treatment of Dirichlet boundary conditions in the transition from the hyperbolic to the parabolic case at outflow boundaries. In the hyperbolic case no boundary condition can be prescribed at outflow boundaries and the numerical method treats the value at the outflow boundary as unknown. If a diffusion term is present a Dirichlet boundary condition is obeyed for $h \rightarrow 0$.

4.2 Runge-Kutta Time Discretizations

Eq. (19) can be rewritten in ODE form after inserting a basis and inverting the mass matrix. The mass matrix is diagonal if an orthogonal basis is chosen (otherwise it is block diagonal). We denote the ODE system by

$$\frac{d}{dt} C_h = L_h(t, C_h(t)). \quad (24)$$

This ODE system is discretized by Runge-Kutta methods. The time interval $(0, T)$ is subdivided into $0 = t^0 < t^1 < \dots < t^M = T$ with $\Delta t^n = t^{n+1} - t^n$. The approximation of $C_h(t)$ to be computed is denoted by C_h^n .

All Runge-Kutta methods used here can be written in the following form which computes C_h^{n+1} from C_h^n :

1. $C_h^{(0)} = C_h^n$;

2. $C_h^{(i)} = \sum_{k=0}^i \left[a_{ik} C_h^{(k)} + b_{ik} \Delta t^n L_h(t^n + d_k \Delta t^n, C_h^{(k)}) \right] \quad i = 1(1)s ;$
3. $C_h^{n+1} = C_h^{(s)} ;$

The number of stages of the scheme is s . Note that schemes with $b_{ii} = 0$ are explicit. Otherwise they are implicit and a large system of nonlinear algebraic equations has to be solved per stage.

For hyperbolic and convection-dominated parabolic problems [35,15] develop explicit schemes with the total variation diminishing (TVD) property. Diagonally implicit Runge-Kutta schemes with favourable stability characteristics are presented in [2,23].

Table 1 displays the coefficients of all schemes used in this work. These are the second and third order explicit TVD methods of [35], the second and third order strongly S-stable methods of [2] and the fourth order L-stable method of [23]. The coefficients are written in the form

$$\begin{array}{cccccc} a_{10} \dots a_{1s} & b_{10} \dots b_{1s} & d_1 & & & \\ \vdots & \vdots & \vdots & \vdots & \vdots & , \quad d_0 = 0. \\ a_{s0} \dots a_{ss} & b_{s0} \dots b_{ss} & d_1 & & & \end{array}$$

The CFL constraint for the explicit schemes is $1/3$ for the second order scheme and $1/5$ for the third order scheme.

Table 1. Coefficients for various explicit and diagonally implicit Runge-Kutta methods.

Reference	Ord. /s	Coefficients											
[35]	2/2	1	0	0	1	0	0	1					
		$\frac{1}{2}$	$\frac{1}{2}$	0	0	$\frac{1}{2}$	0	1					
[35]	3/3	1	0	0	0	1	0	0	0	1			
		$\frac{3}{4}$	$\frac{1}{4}$	0	0	0	$\frac{1}{2}$	0	0	$\frac{1}{2}$			
		$\frac{1}{3}$	0	$\frac{2}{3}$	0	0	0	$\frac{2}{3}$	0	1			
[2]	2/2	1	0	0	0	α	0	α	α	$\alpha = 1 - \frac{\sqrt{2}}{2}$			
		1	0	0	0	$1 - \alpha$	α	1					
[2]	3/3	1	0	0	0	0	α	0	0	α	$\alpha = 0.4358665215$		
		1	0	0	0	0	$\tau_2 - \alpha$	α	0	τ_2	$\tau_2 = (1 + \alpha)/2$		
		1	0	0	0	0	β_1	β_2	α	1	$\beta_1 = -\frac{6\alpha^2 - 16\alpha + 1}{4}$		
											$\beta_2 = \frac{6\alpha^2 - 20\alpha + 5}{4}$		
		1	0	0	0	0	0	$\frac{1}{4}$	0	0	0	$\frac{1}{4}$	
		1	0	0	0	0	0	$\frac{1}{2}$	$\frac{1}{4}$	0	0	$\frac{3}{4}$	
[23]	4/5	1	0	0	0	0	0	$\frac{17}{2}$	$-\frac{1}{4}$	$\frac{1}{4}$	0	0	$\frac{11}{20}$
		1	0	0	0	0	0	$\frac{50}{371}$	$-\frac{25}{137}$	$\frac{1}{15}$	$\frac{1}{4}$	0	$\frac{1}{2}$
		1	0	0	0	0	0	$\frac{1360}{25}$	$-\frac{2720}{48}$	$\frac{544}{125}$	$\frac{1}{4}$	0	$\frac{1}{2}$
		1	0	0	0	0	0	$\frac{25}{24}$	$-\frac{49}{48}$	$\frac{125}{16}$	$-\frac{85}{12}$	$\frac{1}{4}$	1

4.3 Slope Limiters

According to Godunov's theorem [25] there are no monotone linear schemes of order greater than one. Unphysical oscillations in higher order schemes are suppressed by slope limiters. Slope limiters applicable to discontinuous Galerkin space discretizations have been presented in [12,17]. They are incorporated into the Runge-Kutta time-stepping procedure as follows:

1. $C_h^{(0)} = C_h^n$;
2. $C_h^{(i)} = \Lambda\Pi \left(\sum_{k=0}^i \left[a_{ik} C_h^{(k)} + b_{ik} \Delta t^n L_h(t^n + d_k \Delta t^n, C_h^{(k)}) \right] \right)$ $i = 1(1)s$;
3. $C_h^{n+1} = C_h^{(s)}$;

This scheme is called the RK $\Lambda\Pi\Pi$ time-stepping method. $\Lambda\Pi : V^r(E_h) \rightarrow V^r(E_h)$ is a projection that is used to postprocess the solution after each stage such that the TVD property is maintained, for details we refer to [12,17]. $\Lambda\Pi$ is local in the sense that on an element it only uses the solution on that element and in neighboring elements.

We now describe the construction of $\Lambda\Pi$ applied to a function $v \in V^r(E_h)$. Fix a particular element $e \in E_h$. The first step is to extract the linear part v_e^1 on Ω_e through L_2 -projection, i. e.

$$(v_e^1, w)_{\Omega_e} = (v, w)_{\Omega_e} \quad \forall w \in P_1(\Omega_e). \quad (25)$$

$\Lambda\Pi$ relies on the assumption that spurious oscillations in v already show up in its linear part. This is theoretically not proven [17].

In the following we restrict the presentation to the one-dimensional case. The elements are then given by $\Omega_{e_i} = (x_{i-1/2}, x_{i+1/2})$, the center of element e_i is at x_i , $i = 1, \dots, K$. The functions v_{e_i} in $P_1(\Omega_{e_i})$ can be written in the orthonormal basis

$$v_{e_i}^1(x) = \bar{v}_i \phi_{i,0}(x) + \tilde{v}_i \phi_{i,1}(x)$$

with

$$\phi_{i,0}(x) = 1 \quad \text{and} \quad \phi_{i,1}(x) = \frac{x - x_i}{\Delta x_i/2} \quad \text{where} \quad \Delta x_i = x_{i+1/2} - x_{i-1/2}.$$

The two coefficients \bar{v}_i and \tilde{v}_i can be computed from a given $v_{e_i}^1$ by

$$\bar{v}_i = v_{e_i}^1(x_i), \quad \tilde{v}_i = v_{e_i}^1(x_{i+1/2}) - v_{e_i}^1(x_i). \quad (26)$$

Obviously, \bar{v}_i is the average cell value and \tilde{v}_i measures the slope of the linear function. The slope limiter, as the name implies, will possibly modify the slope of the function but not its average value (conservation of mass). The limited slope \tilde{v}_i^* on element e_i is computed by

$$\tilde{v}_i^* = m(\tilde{v}_i, q(\bar{v}_{i+1} - \bar{v}_i), q(\bar{v}_i - \bar{v}_{i-1})) \quad (27)$$

where m is the so-called minmod function

$$m(a_1, a_2, a_3) = \begin{cases} s \min_i |a_i| & \text{if } s = \text{sign}(a_1) = \text{sign}(a_2) = \text{sign}(a_3), \\ 0 & \text{otherwise,} \end{cases}$$

and $q \in (0, 1]$. In (27) the slope on element e_i is compared with the slopes computed from neighboring cell averages. If all slopes have the same sign the slope with the smallest absolute value is selected. Otherwise a local minimum or maximum has been detected and the slope is set to zero. The parameter q is taken as 1 for linear convection and 1/2 for nonlinear convective terms.

In quadrilateral elements two opposite edges define a coordinate direction and the same procedure is applied accordingly. The limiting in case of triangular elements is more complicated and is described in [12,17].

It remains to specify the $\Lambda\Pi$ -projection:

$$\Lambda\Pi(v)|_{\Omega_{e_i}} = \begin{cases} \bar{v}_i \phi_{i,0}(x) + \tilde{v}_i^* \phi_{i,1}(x) & \text{if } \tilde{v}_i^* \neq \bar{v}_i, \\ v|_{\Omega_{e_i}} & \text{else.} \end{cases} \quad (28)$$

5 Numerical Results

The schemes described in this paper have been implemented in the software framework ‘‘Unstructured Grids’’ [6] for the numerical solution of partial differential equations. The implementation covers two- and three-dimensional unstructured meshes and polynomials up to degree 6.

5.1 Multigrid Performance

The convergence of the multigrid solver is illustrated in Tables 2 and 3. For comparison we also list the iteration numbers for regular multigrid applied to a vertex centered finite volume discretization. We use a multigrid V-cycle with one ILU pre- and postsmoothing step and list iteration numbers for a 10^{-8} reduction of the initial residual.

Table 2 shows the iteration numbers for a full regularity model problem $-\Delta p = f$ in $(0, 1)^2$, $p = p_0$ on $\partial\Omega$. A structured quadrilateral mesh with coarse mesh size $h_0 = 1/2$ has been used. Obviously the method is robust in mesh size h and the polynomial degree r .

Multigrid convergence is independent of the regularity of the problem as is shown by Table 3 where a reentrant corner problem with solution in H^s , $s = 1 + 4/7$, has been solved.

5.2 Single Phase Flow in Heterogeneous Media

The second example explores the quality of the DG solutions for elliptic problems with highly discontinuous coefficients. We solve $-\nabla \cdot \{K \nabla p\}$ in the unit square with $p = 1$ for $x = 0$, $p = 0$ for $x = 1$ and no flow boundary

Table 2. Number of multigrid iterations for full regularity model problem.

h^{-1}	FV	$r = 2$	$r = 3$	$r = 4$	$r = 5$	$r = 6$
4	3	5	5	5	5	4
8	4	7	6	6	5	6
16	4	7	6	6	5	6
32	4	7	6	6	5	6
64	4	7	6	6	5	6
128	4	6	6	6		
256	4					
512	4					

Table 3. Number of multigrid iterations for reentrant corner problem.

Triangles	FV	$r = 2$	$r = 3$	$r = 4$	$r = 5$	$r = 6$
20	4	7	8	7	7	8
80	6	8	7	7	8	8
320	6	8	8	7	8	8
1280	6	9	8	7	8	8
5120	7	9	8	7		
20480	7	9				
81920	7					

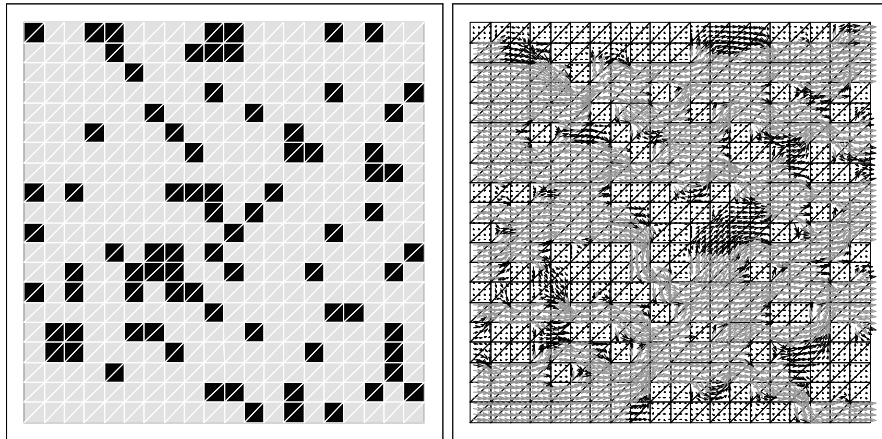


Fig. 1. Permeability and flow field for the discontinuous coefficient example computed with DG(3). Permeability 1 shown in light gray and 10^{-6} in black. Vectors not drawn to scale are indicated by gray color in the vector plot.

conditions for $y = 0$ and $y = 1$. The permeability field is defined on a regular 20×20 mesh and is shown in Fig. 1 on the left. In dark areas the permeability is $K = 10^{-6} \cdot I$, elsewhere it is $K = I$. The example is taken from [19].

The unit square is discretized with $20 \times 20 \times 2$ triangular elements such that the permeability field is resolved with coarse grid elements. Finer grids are obtained through regular refinement. The right plot in Fig. 1 shows the flow field computed with degree $r = 3$ on the coarsest mesh.

Table 4. Total flux through the system for discontinuous coefficient example.

h^{-1}	FV	$r = 2$	$r = 3$	$r = 4$	$r = 5$	$r = 6$	MFE
20	0.6991	0.5094	0.5152	0.5174	0.5232	0.5152	0.4508
40	0.6466	0.5179	0.5181	0.5208	0.5206		
80	0.6170	0.5194	0.5192	0.5201			
160	0.5998	0.5199	0.5198				
320	0.5890						
640	0.5816						

Table 5. Number of multigrid cycles in the discontinuous coefficient example.

l	h^{-1}	FV	$r = 2$	$r = 3$	$r = 4$
1	40	6	14	14	16
2	80	7	14	12	15
3	160	7	13	12	
4	320	8			
5	640	9			

In Table 4 we show results for the unknown total flux through the system. We compare the vertex centered finite volume method (which in this case is identical to P1 conforming finite elements), DG with $r = 2$ up to $r = 6$ and the lowest order mixed finite element method. The value for the mixed method is taken from [19]. The “exact” value has been given in [19] as 0.5205 which was obtained by computing approximations on a sequence of meshes up to 200×200 with a cell centered finite volume scheme and extrapolation to $h = 0$. The results clearly show the unsuitability of the standard finite element method for this type of problem. Moreover, the error in the mixed finite element solution on the coarsest mesh is about a factor six larger than the error in the DG result on the same mesh. However, the number of unknowns is also about 2.5 times larger for DG (4800 vs. 2000 in the non-hybridized version). This result clearly shows the suitability of the DG method since the MFE is considered optimal for this type of problem.

The performance of the multigrid method is shown in Table 5. For the discontinuous coefficient example we used a multigrid V-cycle with $\nu_1 = \nu_2 =$

2 ILU smoothing steps as a preconditioner in the BiCGSTAB-method [36]. The table shows the number of preconditioner evaluations needed to reduce the norm of the defect by 10^{-8} . Again the iteration numbers seem to be independent of h and r .

5.3 Rotating Pulse Problem

In this example we consider the transport of a Gaussian pulse in a rotating flow field. We solve

$$\frac{\partial C}{\partial t} + \nabla \cdot \{uC - D\nabla C\} = 0 \quad \text{in } \Omega = (-0.5, 0.5)^2 \quad (29)$$

with Dirichlet boundary and initial condition taken from the exact solution

$$C(x, y, t) = \frac{2\sigma^2}{2\sigma^2 + 4Dt} \exp\left(-\frac{(\bar{x} - x_c)^2 + (\bar{y} - y_c)^2}{2\sigma^2 + 4Dt}\right) \quad (30)$$

which is available for $u = (-4y, 4x)^T$ and $\bar{x} = x \cos(4t) + y \sin(4t)$, $\bar{y} = -x \sin(4t) + y \cos(4t)$. The exact solution is taken from [37] where many methods are compared for this model problem (unfortunately not in the L_2 norm, only maxima and minima are listed). We use the same parameters as in their paper: $D = 10^{-4}$, $x_c = -0.25$, $y_c = 0$ and $2\sigma^2 = 0.004$. The time interval for the simulation is $[0, \pi/4]$, which is the time for a half rotation. Fig. 2 shows the initial condition and final solution.



Fig. 2. Rotating pulse problem. Initial solution (left) and solution after half rotation (right).

For comparison we list the L_2 error of the solution at $t = \pi/4$ for different methods in Tables 6 and 7. T denotes the number of elements and TS denotes the number of time steps used. Table 6 contains the rates for several

schemes using continuous and piecewise linear trial functions. Spatial and temporal mesh are refined such that $h/\Delta t$ is constant. The backward Euler / full upwinding vertex centered finite volume scheme (column FV BE/FU) is formally of first order. However, the results show that this asymptotic rate is achieved only for very fine meshes requiring huge computational effort. Comparison with the other schemes shows that the asymptotic convergence rate is reached for an absolute error smaller than about $5 \cdot 10^{-3}$. Above that absolute error the observed convergence rate may be much worse than the expected rate. The modified method of characteristic (MMOC) [18] is formally first order convergent but has a small error constant. Asymptotic convergence is achieved already on coarse meshes. The finite volume scheme with Crank-Nicolson time-stepping and central evaluation of convective terms is second-order accurate which is confirmed by the table. It should be noted that the solution is smooth but convection-dominated. The second order scheme shows negligible oscillations on the finer meshes.

Table 7 reports the results for discontinuous Galerkin methods using polynomials of degree 1, 2 and 3 and the corresponding diagonally implicit Runge-Kutta time integrators of order 2, 3 and 4 (see Table 1). The theoretical asymptotic convergence rates are fully confirmed by the table. Since the problem is smooth, no slope limiters are necessary. With respect to efficiency one can state the following: For an accuracy of $5 \cdot 10^{-4}$ even the second order DG scheme is faster than the second order finite volume scheme. The third order DG scheme is about five times faster than the second order scheme, the fourth order scheme is about 12 times faster for a more accurate solution. Computation times in the table are always for the finest mesh using a Pentium III/850 MHz computer.

Table 8 shows results where the DG space discretization is combined with a DG time discretization resulting in a space-time finite element formulation. In this scheme time is treated as a fourth dimension. Upwinding in time naturally leads to a sequential solution of the equation on time slabs, see [20]. This scheme is very competitive with respect to accuracy per computation time. However, it requires more computer memory than the higher order Runge-Kutta schemes which may be prohibitive in practice.

Table 6. Rotating pulse problem. L_2 error after half rotation for some simpler schemes.

h^{-1}	T	TS	MMOC		TS	FV BE/FU		FV CN/CEN	
			Rate	L_2 -Norm		Rate	L_2 -Norm	Rate	L_2 -Norm
8	256				10		$7.24 \cdot 10^{-2}$		$8.87 \cdot 10^{-2}$
16	1K	2		$5.13 \cdot 10^{-2}$	20	0.07	$6.90 \cdot 10^{-2}$	0.22	$7.60 \cdot 10^{-2}$
32	4K	4	0.77	$3.01 \cdot 10^{-2}$	40	0.12	$6.35 \cdot 10^{-2}$	0.47	$5.47 \cdot 10^{-2}$
64	16K	8	0.90	$1.61 \cdot 10^{-2}$	80	0.19	$5.55 \cdot 10^{-2}$	1.11	$2.53 \cdot 10^{-2}$
128	64K	16	0.92	$8.51 \cdot 10^{-3}$	160	0.30	$4.52 \cdot 10^{-2}$	1.74	$7.56 \cdot 10^{-3}$
256	256K	32	0.86	$4.69 \cdot 10^{-3}$	320	0.43	$3.36 \cdot 10^{-2}$	1.96	$1.94 \cdot 10^{-3}$
512	1M				640	0.57	$2.26 \cdot 10^{-2}$	2.00	$4.86 \cdot 10^{-4}$
	comp. time						565 min		384 min

Table 7. Rotating pulse problem. L_2 error after half rotation for the DG schemes.

h^{-1}	T	TS	Order 2		Order 3		Order 4	
			Rate	L_2 -Norm	Rate	L_2 -Norm	Rate	L_2 -Norm
8	256	10		$4.37 \cdot 10^{-2}$		$3.56 \cdot 10^{-2}$		$1.73 \cdot 10^{-2}$
16	1K	20	0.75	$2.59 \cdot 10^{-2}$	1.09	$1.67 \cdot 10^{-2}$	2.69	$2.68 \cdot 10^{-3}$
32	4K	40	1.31	$1.04 \cdot 10^{-2}$	1.86	$4.60 \cdot 10^{-3}$	3.70	$2.05 \cdot 10^{-4}$
64	16K	80	1.83	$2.92 \cdot 10^{-3}$	2.53	$7.91 \cdot 10^{-4}$	3.92	$1.35 \cdot 10^{-5}$
comp. time			21 min		67 min		265 min	

Table 8. Rotating pulse problem. L_2 error after half rotation for space-time DG schemes.

h^{-1}	T	TS	$p = q = 1$		$p = q = 2$		$p = q = 3$	
			Rate	L_2 -Norm	Rate	L_2 -Norm	Rate	L_2 -Norm
8	256	10		$5.53 \cdot 10^{-2}$		$3.29 \cdot 10^{-2}$		$1.61 \cdot 10^{-2}$
16	1K	20	0.65	$3.52 \cdot 10^{-2}$	1.90	$8.77 \cdot 10^{-3}$	3.52	$1.40 \cdot 10^{-3}$
32	4K	40	1.37	$1.36 \cdot 10^{-2}$	3.40	$8.27 \cdot 10^{-4}$	4.80	$5.02 \cdot 10^{-5}$
64	16K	80	2.23	$2.88 \cdot 10^{-3}$	2.51	$7.22 \cdot 10^{-5}$	4.09	$2.94 \cdot 10^{-6}$
comp. time			14 min		42 min		232 min	

5.4 Buckley-Leverett Problem

The Buckley-Leverett problem is an often used test example for two-phase flow without capillary pressure effects in a one-dimensional porous medium. The corresponding equation

$$\frac{\partial S_w}{\partial t} + \frac{u}{\Phi} \frac{\partial}{\partial x} f_w(S_w) = 0 \quad \text{in } (0, 300[m]) \quad (31)$$

for the wetting phase saturation is nonlinear hyperbolic. The fractional flow function

$$f_w(S_w) = \frac{k_{rw}(S_w)}{k_{rw}(S_w) + \frac{\mu_w}{\mu_n} k_{rn}(1 - S_w)} \quad (32)$$

is S -shaped for typical applications. Here we use Brooks-Corey relative permeabilities [24]

$$k_{rw}(S_w) = S_w^{\frac{2+3\lambda}{\lambda}}, \quad k_{rn}(S_n) = S_n^2 \left(1 - (1 - S_n)^{\frac{2+\lambda}{\lambda}} \right) \quad (33)$$

with $\lambda = 2$. The velocity was set to $u = 3 \cdot 10^{-7} [m/s]$, the porosity to $\Phi = 1/5$ and the viscosity ratio was $\mu_w/\mu_n = 1$. The following boundary and initial conditions are imposed:

$$S_w(0, t) = 1, \quad S_w(x, 0) = 0. \quad (34)$$

The analytical solution of this problem can be constructed with the method of characteristics [25,24].

Figure 3 shows the results at the final time $T = 1500[d]$ for polynomial degree 1 and 2 using the explicit TVD Runge-Kutta methods of order 2 and 3 (see Table 1). The CFL number was 0.3 for the second order scheme and 0.18 for the third order scheme. The shock is resolved sharply within about three mesh cells. Experimental orders of convergence in the L_1 and L_2 norm are shown in Table 9. Due to the low regularity of the problem the higher order does not pay off in the shock region. A comparison with standard finite volume methods from [5,7] exhibits that two levels of mesh refinement are needed with the finite volume scheme to match the accuracy of the DG solution.

Table 9. Error and experimental order of convergence of RKDG applied to the Buckley-Leverett problem.

Method	elements	L_1 -error	L_1 -rate	L_2 -error	L_2 -rate
DG(1)	32	$4.41 \cdot 10^{+0}$		$1.06 \cdot 10^{+0}$	
TVD RK(2)	64	$2.40 \cdot 10^{+0}$	0.88	$6.48 \cdot 10^{-1}$	0.71
$Cr = 0.3$	128	$1.37 \cdot 10^{+0}$	0.81	$5.29 \cdot 10^{-1}$	0.29
minmod	256	$7.76 \cdot 10^{-1}$	0.82	$4.38 \cdot 10^{-1}$	0.27
	512	$4.06 \cdot 10^{-1}$	0.93	$2.98 \cdot 10^{-1}$	0.56
DG(2)	32	$3.96 \cdot 10^{+0}$		$9.83 \cdot 10^{-1}$	
TVD RK(3)	64	$2.03 \cdot 10^{+0}$	0.96	$5.89 \cdot 10^{-1}$	0.74
$Cr = 0.18$	128	$1.19 \cdot 10^{+0}$	0.77	$5.02 \cdot 10^{-1}$	0.23
minmod	256	$6.94 \cdot 10^{-1}$	0.78	$4.27 \cdot 10^{-1}$	0.23
	512	$3.58 \cdot 10^{-1}$	0.95	$2.68 \cdot 10^{-1}$	0.67

5.5 McWhorter Problem

For a one-dimensional counter-current two-phase flow the wetting phase saturation S_w can be described by the following doubly degenerate parabolic equation:

$$\Phi \frac{\partial S_w}{\partial t} + \frac{\partial}{\partial x} \left(\frac{\lambda_n \lambda_w}{\lambda_w + \lambda_n} p'_c K \frac{\partial S_w}{\partial x} \right) = 0 \quad \text{in } (0, 1.6[m]) \quad (35)$$

where we recall $\lambda_w(S_w) = k_{rw}(S_w)/\mu_w$, $\lambda_n(S_n) = k_{rn}(S_n)/\mu_n$. The following boundary and initial conditions are imposed:

$$S_w(0, t) = 1, \quad S_w(1.6, t) = 0, \quad S_w(x, 0) = 0. \quad (36)$$

A quasi-analytical solution for this problem has been presented in [26]. Here we use the following parameters: $\Phi = 0.3$, $K = 10^{-10}[m^2]$, $\mu_n = \mu_w = 10^{-3}[Pa \cdot s]$, Brooks-Corey relative permeability functions with $\lambda = 2$ and Brooks-Corey capillary pressure function

$$p_c(S_w) = p_d S_w^{-\frac{1}{\lambda}} \quad (37)$$

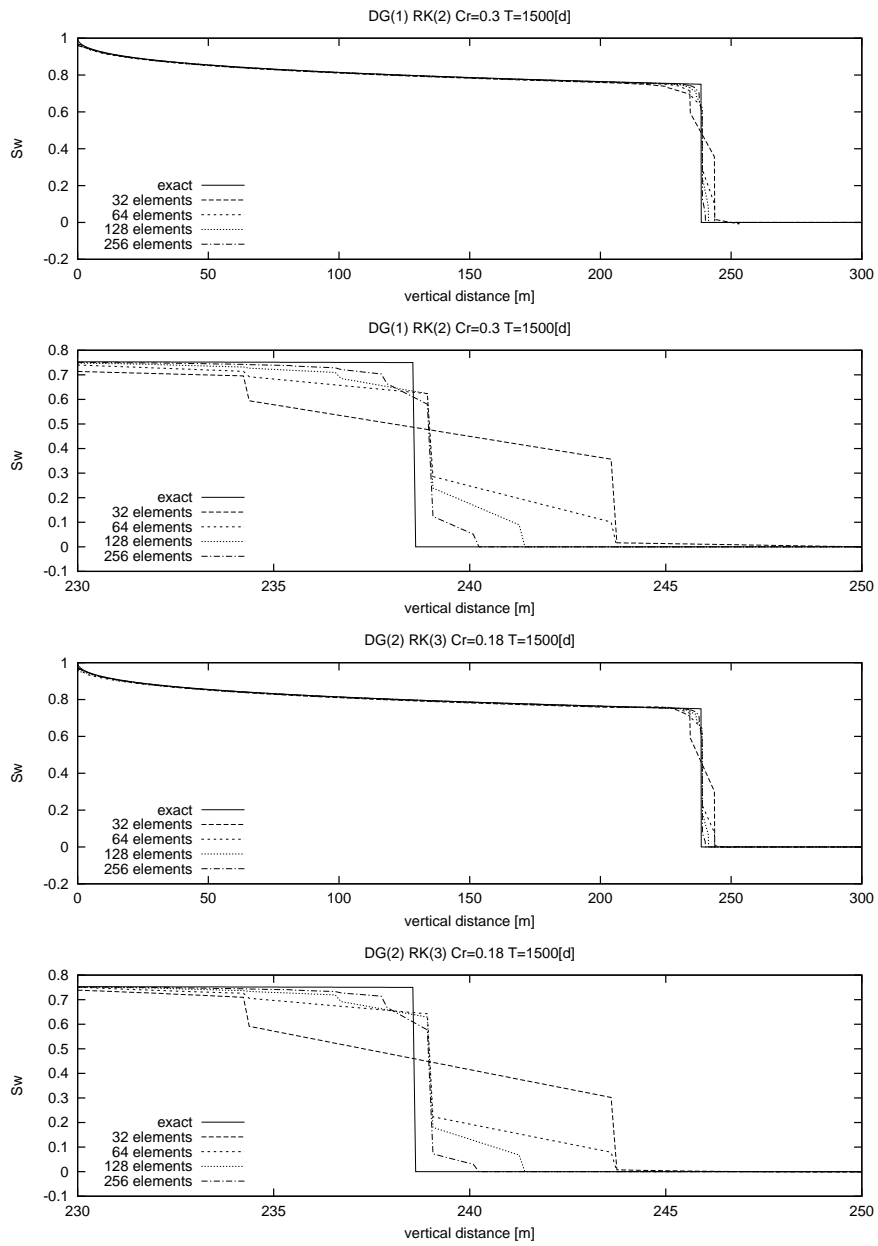


Fig. 3. DG for the Buckley-Leverett problem.

where $\lambda = 2$ and $p_d = 5000[Pa]$.

Solution plots are shown in Figure 4. Because the problem is parabolic we use diagonally implicit Runge-Kutta methods of corresponding order. This problem requires the use of the J_0 penalty term in the saturation equation, otherwise the method does not converge with the initial condition $S_w = 0$ in Ω . The reason for this is that the Oden-Babuška-Baumann stabilization term vanishes for extreme values of saturation. In the J_0 penalty term we use $\sigma = 10^{-3}$ and $\beta = 1$.

The solution of the McWhorter problem does not have enough regularity to realize higher order convergence rates. Nevertheless the much smaller error constant of the higher order schemes renders them very attractive. A comparison of Table 10 with the finite volume method used in [7] shows that the mesh used for the finite volume scheme must be refined three times in space and time to match the accuracy of the DG method.

We observe that the solution for polynomials of degree 2 lies below the exact solution and that for polynomial degree 3 lies above the exact solution.

Table 10. Error and experimental order of convergence of DG applied to the McWhorter problem using implicit Runge-Kutta time discretizations.

Method	elements	steps	L_1 -error	L_1 -rate	L_2 -error	L_2 -rate
DG(2)	16	6	$1.96 \cdot 10^{-2}$		$2.63 \cdot 10^{-2}$	
DIRK(2)	32	12	$1.42 \cdot 10^{-2}$	0.46	$1.98 \cdot 10^{-2}$	0.41
	64	24	$8.98 \cdot 10^{-3}$	0.66	$1.37 \cdot 10^{-2}$	0.53
	128	48	$5.02 \cdot 10^{-3}$	0.84	$8.78 \cdot 10^{-3}$	0.64
DG(3)	16	6	$1.22 \cdot 10^{-2}$		$1.49 \cdot 10^{-2}$	
DIRK(3)	32	12	$7.66 \cdot 10^{-3}$	0.67	$9.37 \cdot 10^{-3}$	0.67
	64	24	$4.79 \cdot 10^{-3}$	0.68	$5.67 \cdot 10^{-3}$	0.72
	128	48	$3.15 \cdot 10^{-3}$	0.60	$3.43 \cdot 10^{-3}$	0.73

6 Conclusion

In this paper we formulated higher order discontinuous Galerkin methods for elliptic, hyperbolic and parabolic equations which describe single-phase and two-phase flow in porous media. For smooth problems the higher-order convergence is fully confirmed. For problems with low regularity it is shown consistently over several examples that the solutions of the presented schemes are very competitive in comparison to other well established methods such as the mixed finite element and finite volume methods. In contrast to the previous approaches with discontinuous elements the new methods allow efficient solution of the arising linear systems with multigrid methods.

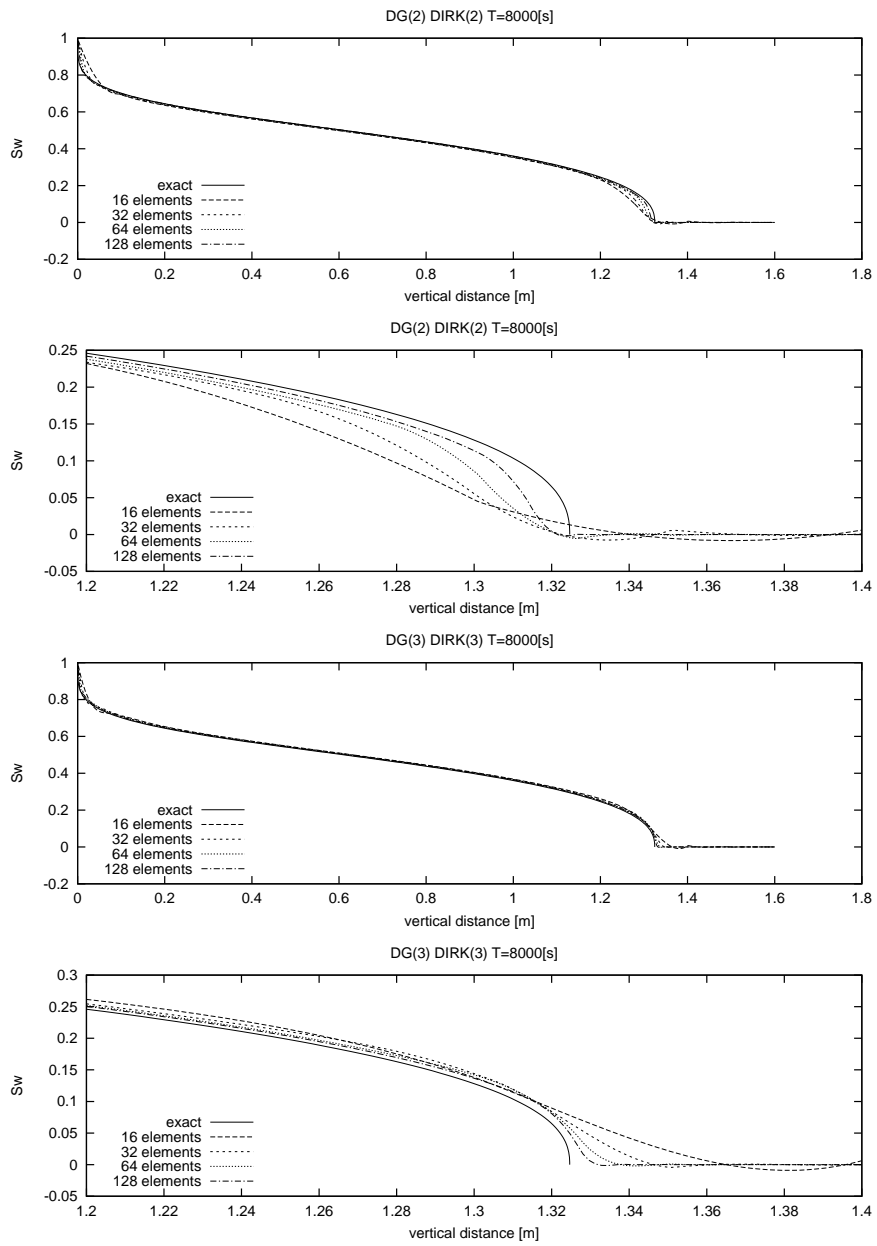


Fig. 4. DG for the McWhorter problem.

References

1. V. Aizinger, C. Dawson, B. Cockburn, and P. Castillo, *The local discontinuous Galerkin method for contaminant transport*, Adv. Wat. Res. **24** (2001), 73–87.
2. R. Alexander, *Diagonally implicit Runge-Kutta methods for stiff O.D.E.'s*, SIAM Journal Numer. Anal. **14** (1977), 1006–1021.
3. D. N. Arnold, F. Brezzi, B. Cockburn, and L. D. Marini, *Unified analysis of discontinuous Galerkin methods for elliptic problems*, SIAM J. Numer. Anal. **39** (2002), no. 5, 1749–1779.
4. K. Aziz and A. Settari, *Petroleum reservoir simulation*, Elsevier, 1979.
5. P. Bastian, *Numerical computation of multiphase flow in porous media*, Habilitationsschrift, , 1999.
6. P. Bastian, K. Birken, S. Lang, K. Johannsen, N. Neuß, H. Rentz-Reichert, and C. Wieners, *UG: A flexible software toolbox for solving partial differential equations*, Computing and Visualization in Science **1** (1997), 27–40, , .
7. P. Bastian and R. Helmig, *Efficient fully-coupled solution techniques for two-phase flow in porous media. Parallel multigrid solution and large scale computations*, Adv. Water Res. **23** (1999), 199–216, .
8. P. Bastian and S. Lang, *Couplex benchmark computations with UG*, Tech. Report 2002–31, IWR (SFB 359), Universität Heidelberg, 2002, , submitted to Computational Geosciences.
9. P. Bastian and V. Reichenberger, *Multigrid for higher order discontinuous Galerkin finite elements applied to groundwater flow*, Tech. Report 2000-37, SFB 359, 2000, .
10. P. Bastian and B. Rivière, *Superconvergence and $H(\text{div})$ -projection for discontinuous Galerkin methods*, Tech. Report 2002-23, IWR (SFB 359), Universität Heidelberg, 2002, , submitted to Int. J. Numer. Meth. Fluids.
11. B. Cockburn, S. Hou, and C.-W. Shu, *TVB Runge-Kutta local projection discontinuous Galerkin finite element method for conservation laws III: One-dimensional systems*, J. Comput. Phys. **84** (1989), 90.
12. ———, *TVB Runge-Kutta local projection discontinuous Galerkin finite element method for conservation laws IV: The multidimensional case*, Math. Comput. **54** (1990), 545.
13. B. Cockburn, S. Y. Lin, and C.-W. Shu (eds.), *Discontinuous Galerkin methods. Theory, computation and applications*, Lecture Notes in Computational Science and Engineering, vol. 11, Springer-Verlag, 2000.
14. B. Cockburn and C.-W. Shu, *TVB Runge-Kutta local projection discontinuous Galerkin finite element method for conservation laws II: Gernerall framework*, Math. Comput. **52** (1989), no. 186, 411–435.
15. ———, *The Runge-Kutta local projection P^1 -discontinuous Galerkin method for scalar conservation laws*, M^2 AN **25** (1991), 337.
16. ———, *The local discontinuous Galerkin finite element method for convection-diffusion systems*, SIAM J. Numer. Anal. **35** (1998), 2440–2463.
17. ———, *The Runge-Kutta discontinuous Galerkin method for conservation laws V: Multidimensional systems*, J. Comput. Phys. **141** (1998), 199–224.
18. J. Douglas Jr. and T. F. Russel, *Numerical methods for convection dominated diffusion problems based on combining the method of characteristics with finite element or finite difference procedures*, SIAM J. Numer. Anal. **19**(5) (1982), 871–885.

19. L. J. Durlofsky, *Accuracy of mixed and control volume finite element approximations to Darcy velocity and related quantities*, *Water Resources Research* **30** (1994), no. 4, 965–973.
20. K. Eriksson, D. Estep, P. Hansbo, and C. Johnson, *Introduction to adaptive methods for differential equations*, *Acta Numerica*, 1995.
21. W. Hackbusch, *Multi-grid methods and applications*, Springer-Verlag, 1985.
22. ———, *Iterative solution of large sparse systems of linear equations*, Springer, 1994.
23. E. Hairer and G. Wanner, *Solving ordinary differential equations II*, Springer, Berlin, 1991.
24. R. Helmig, *Multiphase flow and transport processes in the subsurface – A contribution to the modeling of hydrosystems*, Springer-Verlag, 1997.
25. R. J. LeVeque, *Numerical methods for conservation laws*, Birkhäuser, 1992.
26. D. B. McWhorter and D. K. Sunada, *Exact integral Solutions for two-phase flow*, *Water Resources Research* **26(3)** (1990), 399–413.
27. J. T. Oden, I. Babuška, and C. E. Baumann, *A discontinuous hp finite element method for diffusion problems*, *Journal of Computational Physics* **146** (1998), 491–519.
28. D. W. Peaceman, *Fundamentals of numerical reservoir simulation*, Elsevier, 1977.
29. W. H. Reed and T. R. Hill, *Triangular mesh methods for the neutron transport equation*, Tech. report, Los Alamos Scientific Laboratory, 1973.
30. B. Rivière, *Discontinuous Galerkin methods for solving the miscible displacement problem in porous media*, Ph.D. thesis, The University of Texas at Austin, 2000.
31. B. Rivière and M. F. Wheeler, *Nonconforming methods for transport with nonlinear reaction*, *Fluid Flow and Transport in Porous Media: Mathematical and Numerical* (Z. Chen and R. E. Ewing, eds.), vol. 295, American Mathematical Society, 2002, pp. 421–432.
32. B. Rivière, M. F. Wheeler, and K. Banaś, *Part II. Discontinuous Galerkin method applied to a single phase flow in porous media*, *Comput. Geosci.* **4** (2000), 337–349.
33. B. Rivière, M. F. Wheeler, and V. Girault, *Improved energy estimates for interior penalty, constrained and discontinuous Galerkin methods for elliptic problems I*, *Comput. Geosci.* **3** (1999), 337–360.
34. ———, *A priori error estimates for finite element methods based on discontinuous approximation spaces for elliptic problem*, *SIAM Journal on Numerical Analysis* **39** (2001), no. 3, 902–931.
35. C.-W. Shu, *Total-variation-diminishing time discretizations*, *SIAM J. Sci. Stat. Comput.* **9** (1988), no. 6, 1073–1084.
36. H. A. Van der Vorst, *BiCGSTAB: A fast and smoothly converging variant of Bi-CG for the solution of non-symmetric linear systems*, *SIAM J. Sci. Stat. Comput.* **13** (1992), 631–644.
37. H. Wang, H. K. Dahle, R. E. Ewing, M. S. Espedal, R. C. Sharpley, and S. Man, *An ELLAM scheme for advection-diffusion equations in two dimensions*, *SIAM J. Sci. Stat. Comput.* **20** (1999), no. 6, 2160–2194.
38. M. F. Wheeler, *An elliptic collocation finite element method with interior penalties*, *SIAM J. Numer. Anal.* **15** (1978), no. 1, 152–161.
39. J. Xu, *Iterative methods by space decomposition and subspace correction*, *SIAM Review* **34** (1992), 581–613.